

Structural Behavior of Minrecordite Carbonate Mineral upon Compression: Effect of Mg \rightarrow Zn Chemical Substitution in Dolomite-Type Compounds

David Santamaría-Pérez,* Raquel Chuliá-Jordán, Alberto Otero-de-la-Roza, Javier Ruiz-Fuentes, Julio Pellicer-Porres, and Catalin Popescu



Cite This: *ACS Omega* 2023, 8, 10403–10410



Read Online

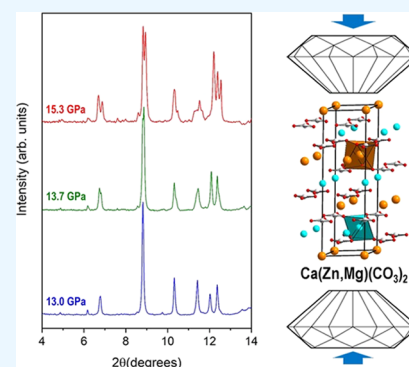
ACCESS |

Metrics & More

Article Recommendations

Supporting Information

ABSTRACT: We report the structural behavior and compressibility of minrecordite, a naturally occurring Zn-rich dolomite mineral, determined using diamond-anvil cell synchrotron X-ray diffraction. Our data show that this rhombohedral $\text{CaZn}_{0.52}\text{Mg}_{0.48}(\text{CO}_3)_2$ carbonate exhibits a highly anisotropic behavior, the c axis being 3.3 times more compressible than the a axis. The axial compressibilities and the equation of state are governed by the compression of the $[\text{CaO}_6]$ and $[\text{ZnO}_6]$ octahedra, which are the cations in larger proportion in each layer. We observe the existence of a dense polymorph above 13.4(3) GPa using Ne as a pressure-transmitting medium, but the onset pressure of the phase transition decreases with the appearance of deviatoric stresses in nonhydrostatic conditions. Our results suggest that the phase transition observed in minrecordite is strain-induced and that the high-pressure polymorph is intimately related to the CaCO_3 -II-type structure. A comparison with other dolomite minerals indicates that the transition pressure decreases when the ratio Zn/Mg in the crystal lattice of pure dolomite is larger than 1. Density functional theory (DFT) calculations predict that a distorted CaCO_3 -II-type structure is energetically more stable than dolomite-type $\text{CaZn}(\text{CO}_3)_2$ above 10 GPa. However, according to our calculations, the most stable structure above this pressure is a dolomite-V-type phase, a polymorph not observed experimentally.



INTRODUCTION

Carbonate minerals are abundant components of the Earth's surface, which are continuously transferred into the interior through subduction processes.¹ These carbonates are thought to be stable phases in the upper mantle, especially in oxidized environments, such as deep subduction zones.² The existence of oxidized carbon species in the lower mantle is also confirmed by carbonate inclusions found in super-deep diamonds.³ Therefore, the knowledge of the phase stability and structural behavior of carbonates at pressures, temperatures, and compositional environments of the inner Earth constitutes essential information to understand the deep carbon cycle.

Ca-containing $\text{CaMg}(\text{CO}_3)_2$ dolomite is one of the principal carbonate minerals in sedimentary rocks.⁴ It is known that dolomite breaks down into the end-member MgCO_3 magnesite and CaCO_3 aragonite carbonates at a pressure of 5–6 GPa and temperatures above 800 K.⁵ Upon cold compression, however, pure $\text{CaMg}(\text{CO}_3)_2$ dolomite is reported to undergo a phase transition at about 20 GPa,⁶ iron-bearing dolomites with compositions $\text{Ca}_{0.988}\text{Mg}_{0.918}\text{Fe}_{0.078}\text{Mn}_{0.016}(\text{CO}_3)_2$ ⁷ and $\text{CaMg}_{0.6}\text{Fe}_{0.4}(\text{CO}_3)_2$ ⁸ are reported to undergo two phase transitions at 17 and 35 GPa, and Fe-rich $\text{Ca}_{1.08}\text{Mg}_{0.24}\text{Fe}_{0.64}\text{Mn}_{0.04}(\text{CO}_3)_2$ ankerite undergoes a transition to a denser phase at 12 GPa.⁹ Results

from high-pressure (HP) laser-heating experiments show that ultradense dolomite does not decompose into the single-cation carbonates up to its melting point (43 GPa, 2600 K).⁸ Besides the different transition pressures, most of the reported X-ray diffraction (XRD) patterns of the high-pressure polymorphs are not compatible between them, evidencing the existence of nonequivalent crystal structures. As observed in other carbonate systems, it is likely that dolomite-type minerals have many polymorphs with similar energies which could crystallize under specific pressure–temperature–composition parameters. In addition to that, density functional theory (DFT) calculations on $\text{CaMg}(\text{CO}_3)_2$ using genetic algorithms predict a distinct thermodynamically stable phase at pressures above 15 GPa, which would suggest that the observed phases are metastable.¹⁰ Both the experimental observations and DFT results indicate that the dolomite group has a complex compositionally dependent P – T energy landscape and that

Received: December 27, 2022

Accepted: January 12, 2023

Published: March 8, 2023



the crystal chemistry of dolomite-type compounds is still poorly known. Further experiments are therefore needed.

Zincian dolomites are more extensively distributed than previously thought.¹¹ A recent investigation carried out in several mining districts reported that dolomite bodies hosting Zn-sulfide ores form Zn-rich dolomites in near-surface, late-stage oxidation processes. The Zn²⁺ cations substitute Mg²⁺ cations in the crystal lattice of pure dolomite, the maximum substitution found in natural samples being approximately 90%.^{12,13} The absence of a dolomite-type compound where magnesium is completely replaced by zinc is in good agreement with thermochemical calculations that predict a maximum Zn content of 85–90%.¹⁴ Zn-rich CaZn_xMg_{1-x}(CO₃)₂ ($x \geq 0.5$) solid solutions are known as minrecordite.

In this study, we conducted in situ high-pressure synchrotron XRD experiments of CaZn_{0.52}Mg_{0.48}(CO₃)₂ minrecordite up to 16 GPa to better understand the role played by the Mg²⁺ to Zn²⁺ cation substitution on the already complex polymorphism of double carbonates,^{15–17} particularly on dolomite group carbonates,^{6–10} at mantle pressures. DFT theoretical calculations on CaZn(CO₃)₂ and CaZn_{0.5}Mg_{0.5}(CO₃)₂ stoichiometries provide information on the phase stability, compressibility, and anisotropy of minrecordite minerals.

EXPERIMENTAL DETAILS

We studied a naturally occurring minrecordite mineral specimen from the Tsumcorp Mine, Tsumeb, Otavi mountains, Namibia (catalog number 1144, Gunnar Färber Minerals). White powder was carefully isolated and characterized at ambient conditions by means of energy-dispersive X-ray (EDX) spectroscopy and XRD. Quantitative chemical analyses show that the composition of the selected sample is Ca_{0.98(4)}Zn_{0.52(3)}Mg_{0.48(4)}(Cu,Mn)_{0.02(2)}(CO₃)₂, nominally CaZn_{0.52}Mg_{0.48}(CO₃)₂. XRD measurements confirmed that the sample has the dolomite-type structure and the aforementioned divalent cations ratio explained well the intensities of the diffraction pattern.

High-pressure angle-dispersive XRD measurements were carried out in the Materials Science and Powder Diffraction (MSPD) station of the ALBA-CELLS synchrotron light source using a monochromatic wavelength of 0.4246 Å and a beam focused to 20 × 20 μm².¹⁸ Diffraction patterns were collected on a Rayonix charge-coupled device (CCD) detector. A precise calibration of the detector parameters was developed with a reference LaB₆ powder for distortion, and integration to conventional 2θ-intensity data was carried out with the Dioptas software.¹⁹ HP experiments were conducted using gas-membrane-driven diamond-anvil cells (DACs) equipped with diamonds with 450 μm diameter culets, a technique that allows compressing materials and characterizing them in situ while compressed.^{20,21} We preindented the stainless steel gasket to 45 μm thickness and drilled a hole of 200 μm in diameter, which served as the pressure chamber. Three HP XRD experimental runs were carried out at room temperature. In the first one, the sample was loaded without a pressure-transmitting medium (PTM) and Cu metal acted as the internal pressure gauge.²² In the second run, the sample was loaded also with copper, but silicone oil was used as PTM. In the third run, high-purity Ne gas was loaded in the DAC by means of a Sanchez Technologies gas loading apparatus, providing a fluid environment up to 4.7 GPa at room

temperature²³ and a quasi-hydrostatic medium up to 16 GPa.²⁴ The shift of the R1 ruby fluorescence peak was used as a pressure gauge in this run, giving pressure accuracies of 0.1 GPa in the studied 0–16 GPa pressure range.²⁵ The equation of state (EOS) of Ne was used as a second pressure gauge above solidification pressure.²⁶ The indexing and refinement of the powder patterns were performed using the Unitcell,²⁷ Powdercell,²⁸ and Fullprof²⁹ program packages.

COMPUTATIONAL DETAILS

Density functional theory (DFT) calculations were carried out using the projector augmented wave (PAW) method³⁰ implemented in the Quantum ESPRESSO program,³¹ version 6.5. We used the PBEsol functional³² and PAW datasets from the pslibrary³³ with the following number of valence electrons: 10 (Ca), 20 (Zn), 6 (O), and 4 (C). A plane-wave cutoff of 100 Ry was used for the Kohn–Sham states, and 1000 Ry was used for the electron density. k-point grids were chosen to achieve an accuracy of 0.1 mRy in the energy and 0.01 GPa in the trace of the stress tensor. The selected k-point grids were 3 × 4 × 2 (CaCO₃-II) and 4 × 4 × 4 (rest of the phases).

Two constant-pressure structural relaxations were carried out on all structures at 0 and 50 GPa. A grid of 41 equally spaced volumes was set up between the resulting equilibrium volumes, and constant-volume relaxations were run to obtain the corresponding equations of state. All relaxations were carried out with tight convergence criteria of 10⁻⁵ Ry in the energies and 10⁻⁴ Ry/b in the forces. The resulting energy–volume data was fitted with polynomial strain averages using the gibbs2^{34,35} program, to yield their stability as a function of pressure and the other thermodynamic properties.

RESULTS AND DISCUSSION

The evolution and stability of the rhombohedral dolomite-type structure of CaZn_{0.52}Mg_{0.48}(CO₃)₂ minrecordite was studied upon room-temperature compression by means of in situ synchrotron X-ray diffraction. This structure, depicted in Figure 1, seems to be stable up to 10 GPa if no PTM is used, but the XRD patterns present such broad peaks that the existence of a phase transition cannot be ruled out (Figure 1S). The structure is stable upon compression up to 10.7(4) GPa when silicone oil is used as a pressure-transmitting medium (Figure 2S) and the range of stability of this initial phase further increases to 13.4(3) GPa when neon, a more hydrostatic medium, is used (Figure 2). This observation is consistent with the well-known experimental fact that the lack of hydrostaticity drives the phase transition to occur at lower pressures.³⁶ For instance, the lattice parameters of rhombohedral minrecordite at 2.5 GPa are $a = 4.7868(11)$ Å and $c = 15.804(6)$ Å, with a unit cell volume of 313.62(14) Å³ ($Z = 3$). The lattice parameters of the dolomite-type unit cell indexations of all of the experimental runs are collected in Tables 1–3.

The evolution of the unit cell volume and lattice parameters with increasing pressure is illustrated in Figures 3 and 4, respectively. The unit cell parameters of the dolomite-type phase decrease smoothly with pressure in all datasets. However, the lack of hydrostatic conditions in the first two runs (from room pressure when no PTM was used, and from ~4 GPa when silicone oil was used as PTM) entails the observation of smaller compressibilities than in the hydrostatic Ne case. In this work, we will use the XRD data measured

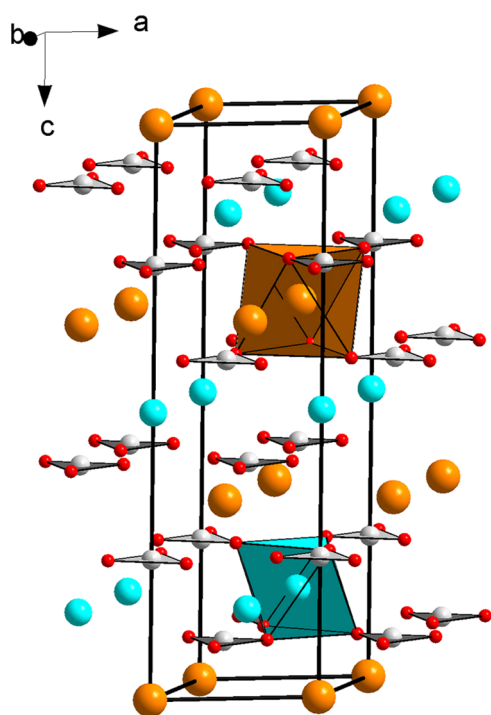


Figure 1. Dolomite-type structure of $R\bar{3}$ rhombohedral minrecordite at ambient pressure. Orange, blue, gray, and red spheres represent Ca, Zn(Mg), C, and O atoms, respectively. It consists of $[\text{CaO}_6]$, $[\text{Zn(Mg)O}_6]$ octahedral units, and trigonal planar $[\text{CO}_3]$ units.

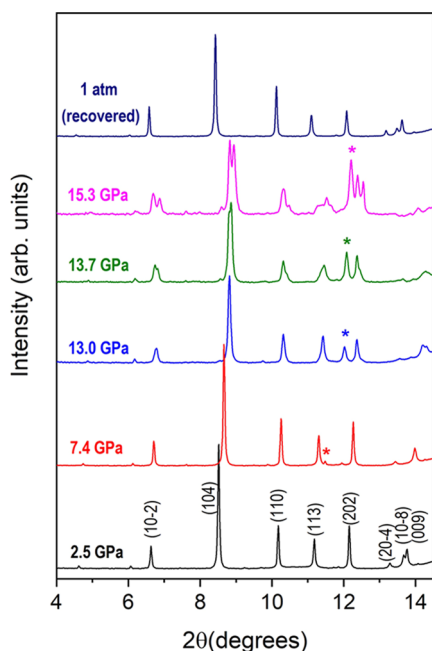


Figure 2. Selected room-temperature X-ray diffraction patterns of minrecordite measured at six different pressures using Ne as pressure-transmitting medium. The neon (111) peak is denoted with an asterisk.

using Ne as PTM and the low-pressure data ($P < 3$ GPa) measured using silicone oil as PTM to estimate the bulk and axial compressibilities of minrecordite. Thus, the axial compressibilities, defined as $\kappa = -1/x(\partial x/\partial P)$ (where $x = a$ or c), estimated from our experimental (theoretical) data are $\kappa_{a0} = 1.50(4) \times 10^{-3} \text{ GPa}^{-1}$ ($1.67(8) \times 10^{-3} \text{ GPa}^{-1}$) and $\kappa_{c0} =$

Table 1. Experimentally Determined Lattice Parameters (a and c) and Unit Cell Volume of $R\bar{3}$ $\text{CaZn}_{0.52}\text{Mg}_{0.48}(\text{CO}_3)_2$ Minrecordite at Different Pressures When No Pressure-Transmitting Medium Is Used^a

pressure (GPa)	a axis (Å)	c axis (Å)	volume (Å ³)
0.0001	4.8095(14)	16.040(19)	321.3(3)
0.05	4.8052(14)	16.060(19)	321.1(3)
0.5	4.8017(14)	16.075(19)	321.0(3)
1.1	4.8019(14)	15.940(19)	318.3(3)
1.8	4.7960(14)	15.909(18)	316.9(3)
2.55	4.7908(14)	15.856(18)	315.2(3)
3.3	4.7854(14)	15.807(18)	313.5(3)
4.2	4.7804(14)	15.753(18)	311.8(3)
5.3	4.7695(14)	15.663(18)	308.6(3)
6.6	4.7617(14)	15.600(18)	306.3(3)
6.9	4.7603(14)	15.584(18)	305.8(3)
10.0	4.7416(14)	15.447(17)	300.8(3)

^aNote that the diffraction peaks were very broad due to deviatoric stresses. This fact could hinder the observation of the high-pressure phase transition above 2 GPa.

Table 2. Experimentally Determined Lattice Parameters (a and c) and Unit Cell Volume of $R\bar{3}$ $\text{CaZn}_{0.52}\text{Mg}_{0.48}(\text{CO}_3)_2$ Minrecordite at Different Pressures Using Silicone Oil as Pressure-Transmitting Medium

pressure (GPa)	a axis (Å)	c axis (Å)	volume (Å ³)
0.1	4.8103(14)	16.041(19)	321.4(3)
0.45	4.8075(15)	16.002(19)	320.3(3)
0.75	4.8048(15)	15.976(19)	319.4(3)
1.85	4.7934(15)	15.875(18)	315.9(3)
2.3	4.7891(15)	15.827(18)	314.4(3)
2.7	4.7852(15)	15.790(18)	313.1(3)
3.2	4.7810(15)	15.744(18)	311.7(3)
3.9	4.7765(15)	15.695(18)	310.1(3)
4.5	4.7726(15)	15.655(18)	308.8(3)
5.4	4.7685(15)	15.576(18)	306.7(3)
6.0	4.7661(15)	15.531(18)	305.5(3)
6.5	4.7652(15)	15.491(18)	304.6(3)
7.2	4.7618(15)	15.434(17)	303.1(3)
7.9	4.7587(15)	15.381(17)	301.6(3)
8.6	4.7566(15)	15.329(17)	300.4(3)
9.5	4.7518(15)	15.265(17)	298.5(3)
10.9	4.7488(15)	15.131(17)	295.5(3)

$5.00(5) \times 10^{-3} \text{ GPa}^{-1}$ ($5.37(7) \times 10^{-3} \text{ GPa}^{-1}$), which evidence the strong anisotropy of this compound. Figure 4 clearly shows that the least compressible axis is the a -axis. This response to external pressure arises from the fact that the relatively incompressible $[\text{CO}_3]$ carbonate units are arranged perpendicular to the c axis, the compressibility of this axis being directly attributable to the compression of the $[\text{CaO}_6]$, $[\text{ZnO}_6]$, and $[\text{MgO}_6]$ octahedra (see Figure 1). The experimental c/a axes ratio follows a linear behavior in the hydrostatic range: $c/a = 3.333(2) - 0.0120(2) \cdot P$ (GPa). This axial behavior is in good agreement with the results of our theoretical calculations: $c/a = 3.3079(11) - 0.0128(1) \cdot P$ (GPa) for a pure $\text{CaZn}(\text{CO}_3)_2$ stoichiometry. The pressure–volume results shown in Figure 3 were analyzed using a third-order Birch–Murnaghan equation of state (EOS), with three fitting parameters: zero-pressure volume (V_0), bulk modulus (B_0), and its first pressure derivative with pressure (B_0').

Table 3. Experimentally Determined Lattice Parameters (*a* and *c*) and Unit Cell Volume of $R\bar{3}$ $\text{CaZn}_{0.52}\text{Mg}_{0.48}(\text{CO}_3)_2$ Minrecordite at Different Pressures Using Neon as Pressure-Transmitting Medium^a

pressure (GPa)	<i>a</i> axis (Å)	<i>c</i> axis (Å)	volume (Å ³)
2.5 (up)	4.7868(11)	15.804(6)	313.62(14)
3.05 (up)	4.7816(11)	15.749(6)	311.83(14)
3.55 (up)	4.7774(11)	15.714(6)	310.58(14)
4.25 (up)	4.7719(11)	15.659(6)	308.80(14)
4.80 (up)	4.7671(13)	15.616(12)	307.32(18)
5.80 (up)	4.7602(13)	15.559(12)	305.32(17)
6.50 (up)	4.7549(13)	15.491(11)	303.32(17)
7.35 (up)	4.7491(13)	15.412(11)	301.04(17)
8.2 (up)	4.7436(13)	15.342(11)	298.96(17)
8.9 (up)	4.7391(13)	15.278(11)	297.16(17)
9.7 (up)	4.7353(13)	15.218(11)	295.52(16)
10.5 (up)	4.7317(13)	15.173(11)	294.18(16)
11.0 (up)	4.7287(13)	15.134(11)	293.08(16)
11.7 (up)	4.7234(13)	15.097(11)	291.70(16)
12.2 (up)	4.7207(13)	15.072(11)	290.88(16)
13.0 (up)	4.7191(14)	15.000(11)	289.30(17)
0.0001 (down)	4.8124(11)	16.058(7)	322.06(15)

^a“Up” and “down” denote upstroke and downstroke pressure measurements, respectively.

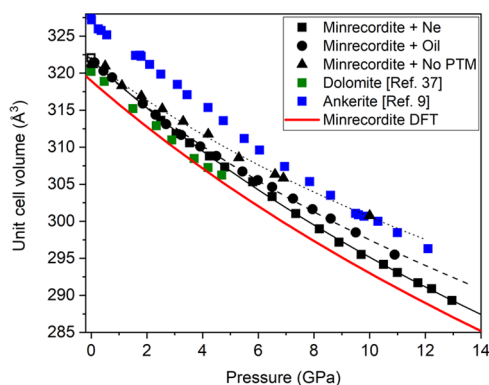


Figure 3. Experimental and calculated pressure dependences of the unit cell volume for the dolomite-type phase of $\text{CaZn}_{0.52}\text{Mg}_{0.48}(\text{CO}_3)_2$ minrecordite. Black squares, circles, and triangles represent the experimental P – V data obtained in this study using Ne, silicone oil, and no PTM, respectively. The solid red line corresponds to our DFT calculations for a pure $\text{CaZn}(\text{CO}_3)_2$ stoichiometry. Green and blue squares are previously reported data of $\text{CaMg}(\text{CO}_3)_2$ dolomite³⁷ and $\text{Ca}_{1.08(6)}\text{Mg}_{0.24(2)}\text{Fe}_{0.64(4)}\text{Mn}_{0.04(1)}(\text{CO}_3)_2$ ankerite,⁹ shown for the sake of comparison.

Experimentally, we find the following characteristic values for $\text{CaZn}_{0.52}\text{Mg}_{0.48}(\text{CO}_3)_2$ minrecordite: $V_0 = 321.85(18) \text{ \AA}^3$, $B_0 = 92(2) \text{ GPa}$, $B_0' = 5.2(4)$ and $V_0 = 321.6(2) \text{ \AA}^3$, $B_0 = 96(4) \text{ GPa}$, $B_0' = 7.5(10)$, when using Ne and silicone oil as pressure media, respectively. Both P – V datasets are compatible until 4 GPa, where the silicone oil data starts to deviate and shows a larger incompressibility with increasing pressure. The dataset corresponding to the experimental run in the absence of PTM differs from quasi-hydrostatic compression data due to deviatoric stresses. Particularly, the compressibility of the *c* axis is significantly smaller (see Figure 4). Our calculations on a pure $\text{CaZn}(\text{CO}_3)_2$ dolomite-type minrecordite yield similar results: $V_0 = 318.91(1) \text{ \AA}^3$, $B_0 = 98.24(12) \text{ GPa}$, $B_0' = 4.31(2)$, as well as the supercell taking into account the stoichiometry

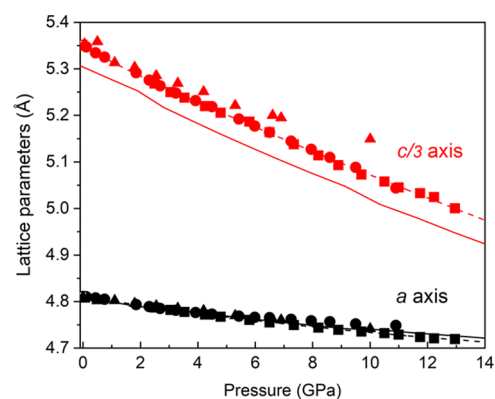


Figure 4. Evolution of the lattice parameters of the dolomite-type phase of $\text{CaZn}_{0.52}\text{Mg}_{0.48}(\text{CO}_3)_2$ minrecordite with pressure. Squares, circles, and triangles represent the experimental P – V data obtained in this study using Ne, silicone oil, and no PTM, respectively. Black and red symbols represent the *a* and *c*/3 axes, respectively. The dashed lines are fits to experimental data using Ne as PTM, and the solid lines correspond to our DFT calculations for a pure $\text{CaZn}(\text{CO}_3)_2$ stoichiometry.

$\text{CaZn}_{0.5}\text{Mg}_{0.5}(\text{CO}_3)_2$: $V_0 = 318.67(6) \text{ \AA}^3$, $B_0 = 94.1(5) \text{ GPa}$, $B_0' = 4.40(6)$. These are the first experimental data on the compressibility of a quaternary compound of the system CaO – ZnO – MgO – CO_2 . The observed compressibility can be compared with that of related calcite-type carbonates ($B_{0,\text{CaCO}_3} = 67(2) \text{ GPa}$, $B_{0,\text{ZnCO}_3} = 124(1) \text{ GPa}$, $B_{0,\text{MgCO}_3} = 107(1) \text{ GPa}$)³⁷ and we conclude, as previously stated for iron-rich ankerite,⁹ that the bulk modulus of minrecordite is approximately the mean of the bulk moduli of the two end-member carbonates with major cation proportion in each layer: $B_0(\text{Ca}_x(\text{Zn,Mg})_{1-x}\text{CO}_3) \sim (B_0(\text{CaCO}_3) + B_0(\text{ZnCO}_3))/2 = (67(2) + 124(1))/2 = 95(2) \text{ GPa}$.

This compressibility behavior is supported by our theoretical calculations. As previously mentioned, we carried out DFT simulations on two different stoichiometries: (i) $\text{CaZn}(\text{CO}_3)_2$ using the $R\bar{3}$ dolomite unit cell, and (ii) $\text{CaZn}_{0.5}\text{Mg}_{0.5}(\text{CO}_3)_2$ using a lower-symmetry triclinic supercell that allows allocating the Zn and Mg atoms within the same layer, as observed experimentally. The relaxed structures at different pressures provide information on the compressibility effects on the $[\text{ZnO}_6]$ and $[\text{CaO}_6]$ octahedra when half of Zn atoms are substituted by Mg atoms. As can be seen in Figure 5, $[\text{CaO}_6]$ octahedra are roughly 2-fold more compressible than $[\text{ZnO}_6]$ octahedra, in good agreement with the bulk moduli experimentally obtained in pure Ca and Zn calcite-type carbonates which are mainly determined by the compression of these units.³⁷ When 50% of the Zn atoms are replaced by Mg atoms, we can appreciate that the $[\text{MgO}_6]$ octahedra are more compressible than those Zn-centered, but the compressibility of $[\text{CaO}_6]$ and $[\text{ZnO}_6]$ does not change significantly. This fact confirms that the compressibility of the layer formed by both $[\text{ZnO}_6]$ and $[\text{MgO}_6]$ octahedra in the fixed $R\bar{3}$ rhombohedral symmetry is mainly determined by the less compressible octahedral units, that is, the $[\text{ZnO}_6]$ octahedra.

The three experimental runs with different and without PTM allow studying the strain-induced peak broadening as a function of increasing pressure. The full width at half-maximum (FWHM) values of five intense diffraction peaks of dolomite-type $\text{CaZn}_{0.52}\text{Mg}_{0.48}(\text{CO}_3)_2$ minrecordite were calculated fitting Lorentzian profiles and subsequently

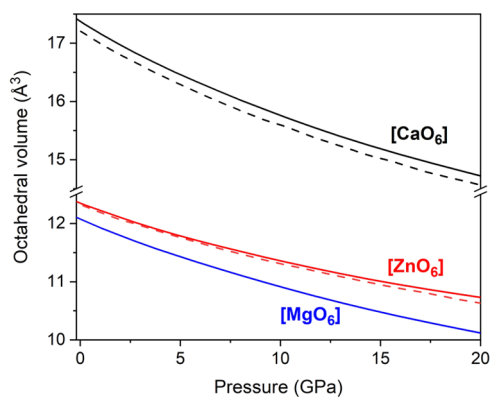


Figure 5. DFT-calculated evolution of the volume of cation-centered octahedra as a function of pressure for dolomite-type $\text{CaZn}(\text{CO}_3)_2$ and $\text{CaZn}_{0.5}\text{Mg}_{0.5}(\text{CO}_3)_2$. Dashed black and red lines correspond to $[\text{CaO}_6]$ and $[\text{ZnO}_6]$ octahedra of $\text{CaZn}(\text{CO}_3)_2$. Solid black, red, and blue lines correspond to $[\text{CaO}_6]$, $[\text{ZnO}_6]$ and $[\text{MgO}_6]$ octahedra of $\text{CaZn}_{0.5}\text{Mg}_{0.5}(\text{CO}_3)_2$, respectively.

subtracting the instrumental broadening (see Figure 6a–c). These peaks are (10 $\bar{2}$), (104), (110), (103), and (202). Since the initial samples of the different experiments come from the same grinding process and the attained top pressure is similar in the three experiments, the average crystalline size was expected to be similar. Therefore, the relative broadening of the diffraction peaks of minrecordite upon compression would be due to lattice strain. Our results evidence the well-known fact that neon is a nearly ideal hydrostatic medium up to 12 GPa,^{24,38} showing no significant peak broadening until this pressure, then increasing rapidly. In silicone oil, the diffraction peaks of the sample continuously broaden with increasing pressure in the studied pressure range. The width of the diffraction peaks of the experimental run without PTM rapidly increases at low pressures, between 0 and 3 GPa, and then the peaks broaden at a lower rate. We interpret the sudden widening of reflections in the Ne run as a signature of the beginning of the displacive phase transition we will discuss below. The phase transition in minrecordite becomes evident in the splitting of the (10 $\bar{2}$) and (104) reflections shown in Figure 2. This transition occurs at $\sim 10.7(4)$ and $\sim 13.4(3)$ GPa for silicone oil and Ne, respectively, when the FWHM values of the diffraction peaks are approximately 0.07–0.10°. This peak width is reached at 1.5–2 GPa when no PTM is used. Surprisingly, a close inspection to the raw XRD images shows splitting of certain peaks at these pressures (see Figure 7), consistent with the proposed high-pressure phase that will be discussed later. These results suggest that the structural distortion associated with the phase transition observed in minrecordite is strain-induced and occurs when deviatoric stresses arise from nonhydrostatic conditions of the pressure-transmitting media.

The XRD patterns of the high-pressure polymorph of $\text{CaZn}_{0.52}\text{Mg}_{0.48}(\text{CO}_3)_2$ minrecordite could not be initially explained by any of the reported post-dolomite structures⁸ nor by the structure of the theoretically predicted more stable phase of dolomite under compression.¹⁰ We index the 10 more intense peaks of the XRD pattern at 15.3 GPa using a monoclinic unit cell with lattice parameters: $a = 5.596(9)$ Å, $b = 4.691(6)$ Å, $c = 7.458(18)$ Å, and $\beta = 103.7(2)^\circ$. These dimensions give a unit cell volume of $190.2(9)$ Å³ that would correspond to two formula units ($Z = 2$). According to this

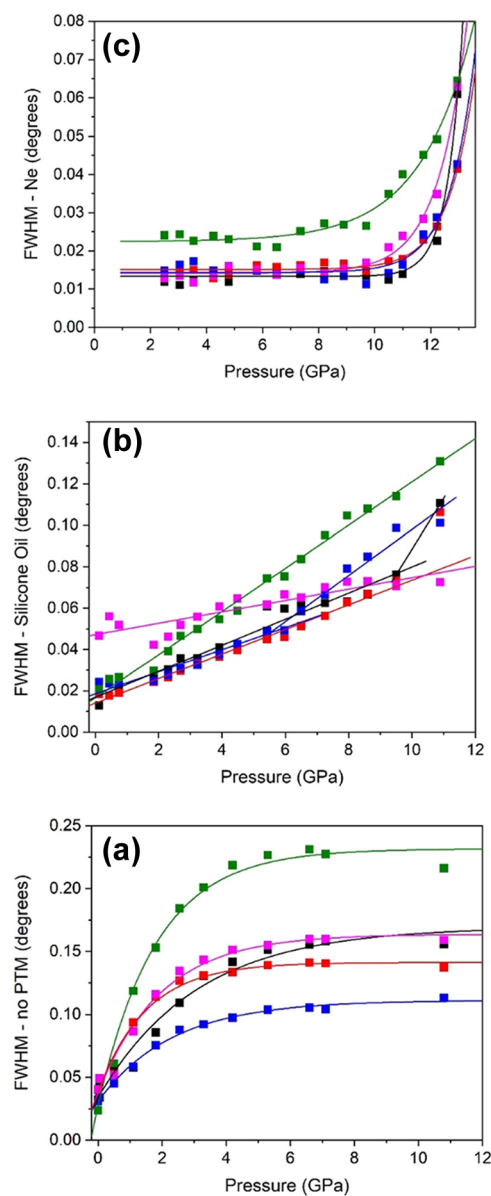


Figure 6. Full width at half-maximum (FWHM) of the (10-2), (104), (110), (103), and (202) diffraction peaks of minrecordite upon compression are represented as black, red, blue, green and magenta squares, respectively. (a), (b) and (c) graphs show the results from experiments using no PTM, silicone oil as PTM and Ne as PTM.

indexation, no volume variation was detected at the transition within experimental accuracy, which would indicate the displacive nature of the transformation. Looking for monoclinic structures of carbonates in the ICSD database, we found that the reported structure of the CaCO_3 -II phase reported by Merrill and Bassett³⁹ has comparable lattice parameters. At 1.8 GPa, CaCO_3 -II is monoclinic with a space group $P2_1/c$ and unit cell dimensions $a = 6.334(20)$ Å, $b = 4.948(15)$ Å, $c = 8.033(25)$ Å, and $\beta = 107.9^\circ$. The XRD pattern profile simulated using the indexed lattice parameters of the HP minrecordite polymorph and the atomic coordinates reported for the CaCO_3 -II phase (where the Ca sites are occupied by Ca, Zn, and Mg according to minrecordite stoichiometry) agrees quite well with the experimentally observed pattern (see Figure 8). Even with such rough approximation, the intensities of most of the diffraction peaks is well explained, which

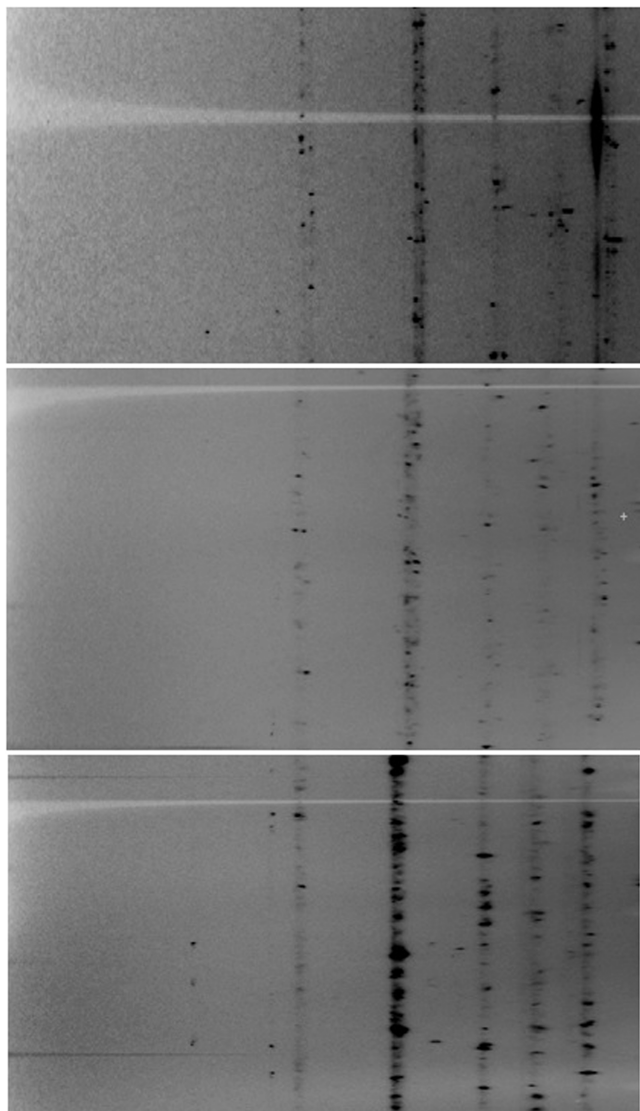


Figure 7. Cake images of the raw data of HP minrecordite at 15.3 GPa using Ne as PTM (top), at 11.9 GPa using silicone oil as PTM (center), and at 2.55 GPa without PTM (bottom).

suggests that minrecordite mineral undergoes a phase transition to a CaCO_3 -II phase when significant deviatoric stresses appear (at 13.4(3) GPa using Ne as PTM). Note, however, that there exist a few unexplained low-intensity peaks that could indicate either a possible coexistence with another HP phase or a lower symmetry of this HP polymorph. In our opinion, this latter explanation is more plausible since the reported experimental $P\bar{1}$ dolomite-II phase in $\text{CaMg}_{0.6}\text{Fe}_{0.4}(\text{CO}_3)_2$ is basically a triclinic distortion of the CaCO_3 -II-type structure.⁸ Unfortunately, the indexations taking into account all of the diffraction peaks were unsuccessful. Assuming that minrecordite undergoes a phase transition to a slightly distorted CaCO_3 -II-type structure upon compression, it is expected to behave similarly to calcium carbonate itself, the transition involving both a slight rotation of the carbonate groups and a small displacement of adjacent planes of cations parallel to the $(10\bar{1}4)$ crystallographic plane of the initial dolomite-type phase. This atomic rearrangement would not lead to a change in the coordination number of metallic atoms, which would remain octahedrally coordinated.

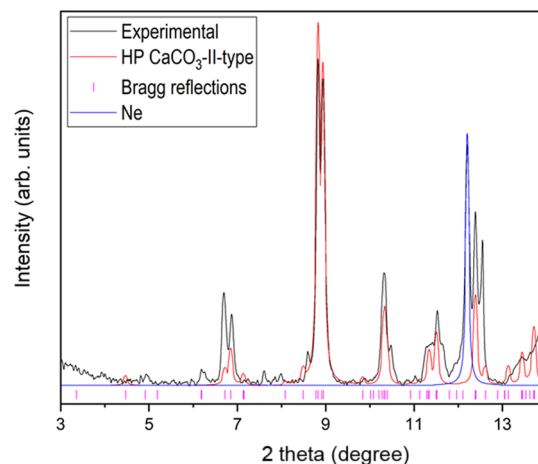


Figure 8. In black, powder X-ray diffraction pattern of $\text{CaZn}_{0.52}\text{Mg}_{0.48}(\text{CO}_3)_2$ post-minrecordite at 15.3 GPa obtained using Ne as PTM. Background is subtracted. Monochromatic synchrotron radiation of wavelength 0.4246 Å was used. The calculated (red) profile of a possible CaCO_3 -II-type³⁹ for the HP phase.

Minrecordite mineral recovers the initial dolomite-type phase after decompression (see Figure 2).

To gain more insight into the stability of the various polymorphs of minrecordite under pressure, we examined the stability of several candidate phases of $\text{CaZn}(\text{CO}_3)_2$ as a proxy for $\text{CaZn}_{0.52}\text{Mg}_{0.48}(\text{CO}_3)_2$ minrecordite. Four phases were studied: the low-pressure minrecordite phase, dolomite-II,⁸ dolomite-V,¹⁰ and the CaCO_3 -II structure³⁹ we propose as the high-pressure phase. The energy–volume and enthalpy–pressure curves for these phases are shown in Figure 9. As

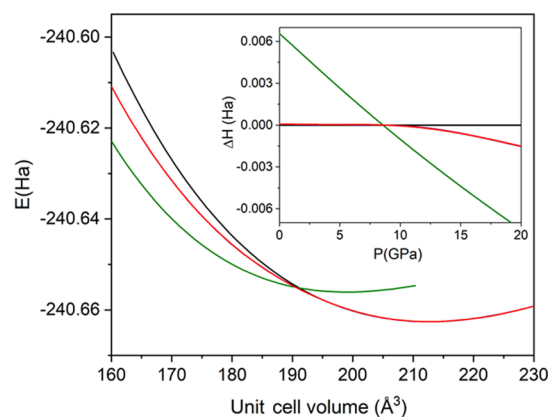


Figure 9. DFT-calculated energy–volume curves for the dolomite-type $\text{CaZn}(\text{CO}_3)_2$ minrecordite phase (black), the dolomite-II- or CaCO_3 -II-type phase (red),^{8,39} and the dolomite-V-type phase (green).¹⁰ Inset: enthalpy difference as a function of pressure, showing the stabilities with respect to $\text{CaZn}(\text{CO}_3)_2$ minrecordite.

expected given their structural similarity, the CaCO_3 -II and dolomite-II phases converge to the same structure at all pressures, effectively being equivalent in the studied pressure range. The phase transition from the low-pressure structure to the CaCO_3 -II phase is predicted to be slightly above 10 GPa and displacive in nature (i.e., no volume change is observed), in good agreement with our XRD data. Surprisingly, the dolomite-V phase is also stabilized at around 10 GPa and is predicted to be the stable phase at high pressure. This phase is not observed in experiment, perhaps because it would involve a

significant structural reconstruction of the material and is therefore kinetically hindered.

CONCLUSIONS

In situ high-pressure synchrotron X-ray diffraction measurements on powder from a natural $\text{CaZn}_{0.52}\text{Mg}_{0.48}(\text{CO}_3)_2$ minrecordite mineral sample show that the stability pressure range of the initial dolomite-type $R\bar{3}$ rhombohedral structure depends on the pressure-transmitting media used in the experiments. Thus, the initial phase is stable up to 13.4(3) and 10.7(4) GPa when Ne and silicone oil were used as pressure media, respectively. This observation confirms the well-known fact that the less hydrostatic the medium is, the lower the transition pressure.³⁶ The absence of pressure-transmitting medium significantly increases deviatoric stresses in the sample and the diffraction peaks broaden even at low pressures. These results suggest that the phase transition observed in minrecordite is strain-induced. At these pressures, rhombohedral minrecordite undergoes a phase transition to a dense polymorph which, according to the XRD data, seems to be intimately related to the CaCO_3 -II-type structure.³⁹ No volume variation apparently takes place at the transition suggesting a displacive transformation, as occurs in the dolomite–dolomite-II (distorted CaCO_3 -II) phase transition itself.⁸ This transition occurs at lower pressures than in Mg-rich iron-bearing $\text{CaMg}_x\text{Fe}_{1-x}(\text{CO}_3)_2$ ($x > 0.5$) dolomite minerals upon room-temperature compression using Ne as the pressure medium, which have transition pressures ranging between 15 and 17 GPa.^{6–8, 40} Fe-rich $\text{Ca}_{1.08}\text{Mg}_{0.24}\text{Fe}_{0.64}\text{Mn}_{0.04}(\text{CO}_3)_2$ ankerite, on the other hand, undergoes a phase transition at 12 GPa.⁹ These experimental observations lead us to suggest that when the amount of Fe atoms, or Zn atoms in our case, substituting Mg in the crystal lattice of pure dolomite exceeds 50%, the onset of the phase transition occurs at lower pressures. More experiments are needed to confirm such hypothesis. DFT calculations predict that the dolomite-II-type structure is energetically more stable than dolomite-type $\text{CaZn}(\text{CO}_3)_2$ above 10 GPa, but also predict that the most stable structure above this pressure is a dolomite-V-type phase which has not been observed experimentally.

The compressibility of the initial rhombohedral minrecordite structure is highly anisotropic, the c axis being approximately 3.3 times more compressible than the a axis. This anisotropy is due to its atomic arrangement. Minrecordite consists of alternating layers of Ca and Zn/Mg atoms interspersed with highly incompressible $[\text{CO}_3]$ carbonate groups oriented normal to the c axis. The compressibility of the c axis and the bulk modulus is therefore basically attributable to the compression of the cation octahedra. Moreover, as a consequence of these alternating $[\text{CaO}_6]$ and $[(\text{Zn}/\text{Mg})\text{O}_6]$ layers in the $R\bar{3}$ symmetry, the bulk modulus is determined by the compressibility of the cation octahedra with major proportion in each layer. That is, in minrecordite, Ca and Zn octahedra. Experimental results give a bulk modulus of $B_0 = 92(2)$ GPa ($B_0' = 5.2(4)$) for minrecordite mineral under hydrostatic compression, which is approximately the mean of the two end-member major carbonates. The aforementioned compressibility and phase transition systematics suggest a dependence of the structural behavior upon compression on both cation composition and deviatoric stresses and should be checked against new experimental data and first-principles simulations.

ASSOCIATED CONTENT

Supporting Information

The Supporting Information is available free of charge at <https://pubs.acs.org/doi/10.1021/acsomega.2c08215>.

XRD patterns of minrecordite mineral measured at different pressures without PTM and using silicone oil as PTM (PDF)

AUTHOR INFORMATION

Corresponding Author

David Santamaría-Pérez – MALTA Consolider Team, Departamento de Física Aplicada-ICMUV, Universitat de València, 46100 Valencia, Spain; orcid.org/0000-0002-1119-5056; Email: David.Santamaria@uv.es

Authors

Raquel Chuliá-Jordán – MALTA Consolider Team, Departamento de Física Aplicada-ICMUV, Universitat de València, 46100 Valencia, Spain; Departamento de Didáctica de las Ciencias Experimentales y Sociales, Universitat de València, 46022 Valencia, Spain; orcid.org/0000-0003-4289-0323

Alberto Otero-de-la-Roza – MALTA Consolider Team, Departamento de Química Física y Analítica, Facultad de Química, Universidad de Oviedo, 33006 Oviedo, Spain; orcid.org/0000-0002-6334-3516

Javier Ruiz-Fuertes – MALTA Consolider Team, DCITIMAC, Universidad de Cantabria, 39005 Santander, Spain; orcid.org/0000-0003-3175-7754

Julio Pellicer-Porres – MALTA Consolider Team, Departamento de Física Aplicada-ICMUV, Universitat de València, 46100 Valencia, Spain; orcid.org/0000-0002-4288-900X

Catalin Popescu – CELLS-ALBA Synchrotron Light Facility, 08290 Barcelona, Spain

Complete contact information is available at: <https://pubs.acs.org/doi/10.1021/acsomega.2c08215>

Notes

The authors declare no competing financial interest.

ACKNOWLEDGMENTS

The authors thank the financial support from the Spanish Ministerio de Ciencia e Innovación (MICINN) and the Agencia Estatal de Investigación under projects MALTA Consolider Ingenio 2010 network (RED2018-102612-T), PID2019-106383GB-C41 and PGC2021-125518NB-I00 (co-financed by EU FEDER funds), and from the Generalitat Valenciana under projects CIAICO/2021/241, CIPROM/2021/075 and MFA/2022/007 (funded by the European Union-Next Generation EU). A.O.-d.-l.-R. acknowledges the financial support of the Spanish MINECO RyC-2016-20301 Ramón y Cajal Grant. The authors also thank the MALTA Consolider supercomputing center and Compute Canada for computational resources and ALBA-CELLS synchrotron for providing beamtime under experiments 2020084419 and 2021024988. These experiments were performed at the MSPD beamline with the collaboration of ALBA staff.

REFERENCES

(1) Dasgupta, R. Ingassing, storage, and outgassing of terrestrial carbon through geologic time. *Rev. Mineral. Geochem.* **2013**, *75*, 183.

- (2) Dasgupta, R.; Hirschmann, M. M. The deep carbon cycle and melting in Earth's interior. *Earth Planet. Sci. Lett.* **2010**, *298*, 1–13.
- (3) Brenker, F. E.; Vollmer, C.; Vincze, L.; Vekemans, B.; Szymanski, A.; Janssens, K.; Szaloki, I.; Nasdala, L.; Joswig, W.; Kaminsky, F. Carbonates from the lower part of transition zone or even lower mantle. *Earth Planet. Sci. Lett.* **2007**, *260*, 1.
- (4) Mackenzie, F. T. In *Carbonate Mineralogy and Geochemistry In Encyclopedia of Sediments and Sedimentary Rocks*; Middleton, G. V.; Church, M. J.; Coniglio, M.; Hardie, L. A.; Longstaffe, F. J., Eds.; Encyclopedia of Earth Sciences Series; Springer: Dordrecht, 1978; pp 93–100.
- (5) Shirasaka, M.; Takahashi, E.; Nishihara, Y.; Matsukage, K.; Kikegawa, T. In situ X-ray observation of the reaction dolomite = aragonite + magnesite at 900–1300 K. *Am. Mineral.* **2002**, *87*, 922–930.
- (6) Santillán, J.; Williams, Q.; Knittle, E. Dolomite-II: A high-pressure polymorph of $\text{CaMg}(\text{CO}_3)_2$. *Geophys. Res. Lett.* **2003**, *30*, No. 1054.
- (7) Mao, Z.; Armentrout, M.; Rainey, E.; Manning, C. E.; Dera, P.; Prakapenka, V. B.; Kavner, A. Dolomite-III: A new candidate lower mantle carbonate. *Geophys. Res. Lett.* **2011**, *38*, No. L22303.
- (8) Merlini, M.; Crichton, W. A.; Hanfland, M.; Gemmi, M.; Müller, H.; Kupenko, I.; Dubrovinsky, L. Structures of dolomite at ultrahigh pressure and their influence on the deep carbon cycle. *Proc. Natl. Acad. Sci. U.S.A.* **2012**, *109*, 13509–13514.
- (9) Chuliá-Jordán, R.; Santamaria-Perez, D.; Ruiz-Fuertes, J.; Otero-de-la-Roza, A.; Popescu, C. Compressibility and phase stability of iron-rich ankerite. *Minerals* **2021**, *11*, No. 607.
- (10) Solomatova, N. V.; Asimow, P. D. Ab initio study of the structure and stability of $\text{CaMg}(\text{CO}_3)_2$ at high pressure. *Am. Mineral.* **2017**, *102*, 210–215.
- (11) Boni, M.; Mondillo, N.; Balassone, G. Zincian dolomite: A peculiar dedolomitization case? *Geology* **2011**, *39*, 183–186.
- (12) Garavelli, C. G.; Vurro, F.; Fioravanti, G. C. Minrecordite, a new mineral from Tsumeb. *Mineral. Rec.* **1982**, *13*, 131–136.
- (13) Rosenberg, P. E.; Champness, P. E. Zincian dolomites and associated carbonates from the Warynski mine, Poland: An AEM investigation. *Am. Mineral.* **1989**, *74*, 461–465.
- (14) Rosenberg, P. E.; Foit, F. F., Jr. The stability of transition metal dolomites in carbonate systems: a discussion. *Geochim. Cosmochim. Acta* **1979**, *43*, 951–955.
- (15) Santamaria-Perez, D.; Otero-de-la-Roza, A.; Ruiz-Fuertes, J.; Chulia-Jordan, R.; Marqueño, T.; MacLeod, S.; Popescu, C. Pressure and temperature effects on low-density $\text{Mg}_3\text{Ca}(\text{CO}_3)_4$ huntite carbonate. *J. Phys. Chem. C* **2020**, *124*, 1077–1087.
- (16) Chuliá-Jordán, R.; Santamaria-Perez, D.; Ruiz-Fuertes, J.; Otero-de-la-Roza, A.; Popescu, C. Crystal structure of $\text{BaCa}(\text{CO}_3)_2$ alstonite carbonate and its phase stability upon compression. *ACS Earth Space Chem.* **2021**, *5*, 1130–1139.
- (17) Chuliá-Jordán, R.; Santamaria-Perez, D.; Gonzalez-Platas, J.; Otero-de-la-Roza, A.; Ruiz-Fuertes, J.; Popescu, C. Phase stability and dense polymorph of the $\text{BaCa}(\text{CO}_3)_2$ barytocalcite carbonate. *Sci. Rep.* **2022**, *12*, No. 7413.
- (18) Fauth, F.; Peral, I.; Popescu, C.; Knapp, M. The new material science powder diffraction beamline at ALBA synchrotron. *Powder Diffr.* **2013**, *28*, S360.
- (19) Prescher, C.; Prakapenka, V. B. DIOPTAS: A Program for Reduction of Two-Dimensional X-Ray Diffraction Data and Data Exploration. *High Pressure Res.* **2015**, *35*, 223–230.
- (20) Santamaria-Perez, D.; Garbarino, G.; Chulia-Jordan, R.; Dobrowolski, M. A.; Muehle, C.; Jansen, M. Pressure-induced phase transformations in mineral chalcocite, Cu_2S , under hydrostatic conditions. *J. Alloys Compd.* **2014**, *610*, 645–650.
- (21) Santamaria-Perez, D.; McGuire, C.; Makhluif, A.; Kavner, A.; Chulia-Jordan, R.; Jorda, J. L.; Rey, F.; Pellicer-Porres, J.; Martinez-Garcia, D.; Rodriguez-Hernandez, P.; Muñoz, A. Correspondence: Strongly-driven $\text{Re} + \text{CO}_2$ redox reaction at high-pressure and high-temperature. *Nat. Commun.* **2016**, *7*, No. 13647.
- (22) Dewaele, A.; Loubeyre, P.; Mezouar, M. Equations of state of six metals above 94 GPa. *Phys. Rev. B* **2004**, *70*, No. 094112.
- (23) Santamaria-Pérez, D.; Mukherjee, G. D.; Schwager, B.; Boehler, R. High-pressure melting curve of helium and neon: Deviations from corresponding states theory. *Phys. Rev. B* **2010**, *81*, No. 214101.
- (24) Klotz, S.; Chervin, J. C.; Munsch, P.; Le Marchand, G. Hydrostatic limits of 11 pressure transmitting media. *J. Phys. D: Appl. Phys.* **2009**, *42*, No. 075413.
- (25) Mao, H. K.; Xu, J.; Bell, P. M. Calibration of the ruby pressure gauge to 800 Kbar under quasi-hydrostatic conditions. *J. Geophys. Res.* **1986**, *91*, 4673.
- (26) Hemley, R. J.; Zha, C. S.; Jephcoat, A. P.; Mao, H. K.; Finger, Cox, D. E. L. W. X-ray diffraction and equation of state of solid neon to 110 GPa. *Phys. Rev. B* **1989**, *39*, 11820–11827.
- (27) Holland, T. J. B.; Redfern, S. A. T. Unit cell refinement from powder diffraction data: the use of regression diagnostics. *Mineral. Mag.* **1997**, *61*, 65–77.
- (28) Nolze, G.; Kraus, W. Powdercell 2.0 for Windows. *Powder Diffr.* **1998**, *13*, 256–259.
- (29) Rodríguez-Carvajal, J. Recent advances in magnetic structure determination by neutron powder diffraction. *Phys. B* **1993**, *192*, 55–69.
- (30) Blöchl, P. E. Projector augmented-wave method. *Phys. Rev. B* **1994**, *50*, 17953.
- (31) Giannozzi, P.; Andreussi, O.; Brumme, T.; et al. Advanced capabilities for materials modelling with Quantum ESPRESSO. *J. Phys.: Condens. Matter* **2017**, *29*, No. 465901.
- (32) Perdew, J. P.; Ruzsinszky, A.; Csonka, G.; Vydrov, O. A.; Scuseria, G. E.; Constantin, L. A.; Zhou, X.; Burke, K. Restoring the density-gradient expansion for exchange in solids and surfaces. *Phys. Rev. Lett.* **2008**, *100*, No. 136406.
- (33) Dal Corso, A. Pseudopotentials periodic table: From H to Pu. *Comput. Mater. Sci.* **2014**, *95*, 337–350.
- (34) Otero-de-la-Roza, A.; Luaña, V. Gibbs2: A new version of the quasi-harmonic model code. I. Robust treatment of the static data. *Comput. Phys. Commun.* **2011**, *182*, 1708–1720.
- (35) Otero-de-la-Roza, A.; Abbasi-Perez, D.; Luaña, V. Gibbs2: A new version of the quasi-harmonic model code. II. Models for solid-state thermodynamics, features and implementation. *Comput. Phys. Commun.* **2011**, *182*, 2232–2248.
- (36) Santamaria-Pérez, D.; Gracia, L.; Grabarino, G.; Beltrán, A.; Chulia-Jordan, R.; Gomis, O.; Errandonea, D.; Ferrer-Roca, C.; Martínez-García, D.; Segura, D. High-pressure study of the behavior of mineral barite by X-ray diffraction. *Phys. Rev. B* **2011**, *84*, No. 054102.
- (37) Zhang, J.; Reeder, R. J. Comparative compressibilities of calcite-structure carbonates: Deviations from empirical relations. *Am. Mineral.* **1999**, *84*, 861–870.
- (38) Santamaria-Perez, D.; Ruiz-Fuertes, J.; Peña-Alvarez, M.; Chulia-Jordan, R.; Marqueño, T.; Zimmer, D.; Gutierrez-Cano, V.; MacLeod, S.; Gregoryanz, E.; Popescu, C.; Rodriguez-Hernandez, P.; Muñoz, A. Post-tilleyite, a dense calcium silicate-carbonate phase. *Sci. Rep.* **2019**, *9*, No. 7898.
- (39) Merrill, L.; Bassett, W. A. The crystal structure of $\text{CaCO}_3(\text{II})$, a high-pressure metastable phase of calcium carbonate. *Acta Crystallogr., Sect. B: Struct. Crystallogr. Cryst. Chem.* **1975**, *31*, 343–349.
- (40) Zhao, Ch.; Xu, L.; Gui, W.; Liu, J. Phase stability and vibrational properties of iron-bearing carbonates at high pressure. *Minerals* **2020**, *10*, No. 1142.